Korean Chem. Eng. Res., 61(4), 627-634 (2023)
https://doi.org/10.9713/kcer.2023.61.4.627
PISSN 0304-128X, EISSN 2233-9558

Platinum Decoration of a 3D Oxidized Graphitic Carbon Nitride/Graphene Aerogel for Enhanced Visible-Light Photocatalytic Hydrogen Evolution

Thi Kieu Oanh Nguyen, Thanh Truong Dang, Tahereh Mahvelati-Shamsabadi and Jin Suk Chung†

Chemical Engineering, University of Ulsan 93 Daehak-ro, Nam-gu, Ulsan 44610, Korea
(Received 18 July 2023; Received in revised from 16 August 2023; Accepted 16 August 2023)

Abstract – Graphitic carbon nitride (g-C_3N_4) has attracted considerable attention since its discovery for its catalysis of water splitting to hydrogen and oxygen under visible light irradiation. However, pristine g-C_3N_4 confers only low photocatalytic efficiency and requires surface cocatalysts to reach moderate activity due to a lack of accessible surface active sites. Inspired by the high specific surface area and superior electron transfer of graphene, we developed a strongly coupled binary structure of graphene and g-C_3N_4 aerogel with 3D porous skeleton. The as-prepared 3D structure photocatalysts achieve a high surface area that favors efficient photogenerated charge separation and transfer, enhances the light-harvesting efficiency, and significantly improves the photocatalytic hydrogen evolution rate as well. The photocatalyst performance is observed to be optimized at the ratio 3:7 (g-C_3N_4:GO), leading to photocatalytic H_2 evolution of 16125.1 mmol. g^{-1}. h^{-1} under visible light irradiation, more than 161 times higher than the rate achieved by bulk g-C_3N_4.

Key words: Graphitic carbon nitride, Graphene, 3D aerogel, Hydrogen evolution, High surface area

1. Introduction

For human existence, social civilization, and economic growth, energy is an essential commodity. Long-term usage of traditional fossil fuels like coal, petroleum, and natural gas has led to tremendous energy consumption, uncontrolled extraction, and waste; these nonrenewable resources are on the verge of running out. The issue of the energy crisis has gotten worse, in particular due to the continued growth of the world's population and the fast development of economies [1]. Furthermore, the use, misuse and excessive exploitation of fossil fuels have seriously polluted the ecosystem. Therefore, most nations are eager to discover a viable substitute for traditional energy sources [2,3].

Much attention has been given to photocatalytic water splitting under solar irradiation for the green synthesis of renewable hydrogen from water. In the water splitting reaction, Gibbs free energy increases by 237 kJ mol^{-1}, making it an uphill reaction. Light, ideally in the form of sunlight, provides the energy for photocatalytic water splitting. Bandgap excitation causes electrons and holes to form inside semiconductor photocatalyst particles, followed by transfer to surface active sites, where photoexcited carriers are then consumed by surface redox processes. Thus, accessible active sites are crucial to achieving maximized photoactivity of a photocatalyst.

Creation of 3D graphene-based architecture has enabled further improvement of catalytic activity from several perspectives: improved mechanical stability, a larger surface area to accommodate many catalytically active sites, a multidimensional conductive network for efficient electron transport, and a larger space to enhance mass transfer through the catalyst.

Graphitic carbon nitride (g-C_3N_4) is a 2D layered semiconductor resembling graphite that is made up of organized tri-s-triazine subunits, which are joined by planar tertiary amino groups inside of each layer; weak van der Waals interaction exists between layers [4]. The g-C_3N_4 powder has thus emerged as a suitable source for manufacturing free-standing monolayers of g-C_3N_4 nanosheets using liquid or thermal exfoliation techniques. In addition to their inherent properties, two-dimensional (2D) g-C_3N_4 nanosheets (2D-CN) exhibit several unique characteristics, including high surface area, large aspect ratios, and ultrahigh nitrogen content [5]. These characteristics make them excellent candidates to serve as building blocks for 3D architecture with extremely high nitrogen content. However, the intrinsically porous microstructure of these materials results in low electrical conductivity, which severely degrades their chemical capability restricting their use in photocatalysis [6]. As an arranged monolayer of carbon atoms, graphene has many unusual features, including excellent electrical conductivity, a large surface area, excellent mechanical flexibility, and high thermal stability [7]. Thus, nanocomposites based on graphene can be used in a wide variety of applications.

In this work, a method for mass production of graphene-based g-C_3N_4 nanosheets (Pt-3DCN-GO) was developed. The resultant 3D structures retain the high electrical conductivity of all catalysts and provide large, accessible, multi-size holes for rapid delivery of

† To whom correspondence should be addressed.
E-mail: jschung@ulsan.ac.kr

reactants to the redox active sites. Because of this, Pt-3DCN-GO architectures exhibit excellent photocatalytic properties that are superior to those of 2D-CN hybrids when used as H_2 evolution photocatalysts, including exceptional photocatalytic activity, unusual poison tolerance, and reliable stability.

2. Experiment

2-1. Materials

Graphite oxide was purchased from Standard Graphene, Korea. Dicyandiamide (DCDA), triethanolamine (TEOA), sulfuric acid (H_2SO_4), potassium dichromate ($K_2Cr_2O_7$), and chloroplatinic acid (H_2PtCl_6) were purchased from Sigma Aldrich. Eosin Y and organic solvents were purchased from Samchun Chemicals, Korea. Highly pure argon gas was purchased from the MS Gas Corporation, Korea. All chemicals were used as received without further purification.

2-2. Synthesis of 3D-CN-G aerogel

2-2-1. Synthesis of the bulk graphitic carbon nitride (CNb)

The bulk form of graphitic carbon nitride was prepared through a solid-state polymerization of dicyandiamide (DCDA). In particular, 10 g of DCDA was placed in a rectangular crucible with a cover and heated in air atmosphere at 550 ℃ for 4 h in a furnace with a ramp rate of 3 ℃ min^{-1}. After cooling naturally, the obtained yellow product was collected and fully ground, yielding the powder sample denoted as CNb.

2-2-2. Synthesis of 2D oxidized graphitic carbon nitride nanosheets (2D-oCN)

2D oxidized graphitic carbon nitride was synthesized by chemical oxidation of the bulk g-C_3N_4 (CNb) in a mixture of $K_2Cr_2O_7/H_2SO_4$ solution [8]. In particular, 10 g of $K_2Cr_2O_7$ was mixed with 50 mL of H_2SO_4 (98 wt%) in a 100 mL flask and stirred until the solution became brown. Then, 0.5 g of CNb was added into the solution and stirred thoroughly for 2 h at room temperature. The mixture was slowly poured into 400 mL of deionized water and cooled to room temperature. After filtration and washing thoroughly with deionized water to remove all residual acids, the remaining pale yellow solid was dispersed in water and sonicated for1 h. Finally, the obtained milky solution was labeled as 2D-oCN.

2-2-3. Synthesis of 3D-CN-G aerogel

The 3D-CN-G composites with different loading ratios of graphitic carbon nitride and graphene oxide (oCN:GO) of 9:1, 7:3, 5:5, 3:7, 1:9 were synthesized. In a typical synthesis route for the feeding ratio of oCN:GO of 5:5, 5 ml of GO suspension (6 mg/mL) was mixed with 5 mL of 2D-oCN dispersion (6 mg/mL). The mixture was sonicated for 0.5 h and then ethylene diamine (EDA, 20 μL) was added as a linker. The mixture was heated at 95 ℃ for 6 h to create a hydrogel-like precipitant. In the next step, the as-prepared hydrogel system was cooled using liquid nitrogen and then freeze-dried for 72 h. During this step, solvents were totally removed and 3D-CN-GO was generated. Finally, to convert graphene oxide in the 3D structure into reduced graphene oxide (RGO), 3D-CN-GO was reduced using pure H_2 gas at 200 ℃ for 2 h in a tubular furnace and the final product denoted as 3D-CN5-G5. For comparison, the other 3D samples of 3DCN9-G1, 3DCN7-G3, 3DCN5-G5, 3DCN3-G7, 3DCN1-G9 were synthesized with similar methodology.

2-3. H_2 evolution performance measurement

Photocatalytic H_2 evolution under visible-light irradiation in a quartz flask reactor (volume: 300 mL, diameter: 70 mm, and height: 80 mm, surrounded by a water jacket as cooling system) was implemented by a 300 W xenon light source (MAX350, Ashasi. UV Filter cutoff, $\lambda > 420$ nm). The focused intensity of the light on the solution was 100 mW cm^{-2}. Specifically, 20 mg of the as-prepared catalyst (dispersed in 50 mL DI water) was added into the quartz reactor, followed by 20 mg of Eosin Y as a photosensitizer, and then sonication was applied for 30 min at RT to form a homogeneous dispersion. 20 mL of TEOA solution was added to the reactor as a sacrificial agent, and the system was purged with highly pure argon gas for 10 min to flush out the air from the system. A certain amount of an aqueous solution of $H_2PtCl_6 \cdot 6H_2O$ (3 wt% of Pt based on the catalyst weight) was then added to the dispersion and mixed for 15 min. The system was purged with highly pure argon gas for 10 min to flush out the air. Then, the dispersion was irradiated for 2 h and the system was maintained with Ar gas flow. After that, the irradiation continued and the evolved H_2 gas was measured via an automatic injection, online gas chromatographer with a thermal conductive detector (TCD), and a Carboxen 1000 column (Sigma-Aldrich).

2-4. Characterization

The elemental composition of the samples was analyzed using an elemental analyzer (Flash 2000, Thermo Scientific). Scanning electron microscopy (SEM; JSM-600F JEOL, Tokyo, Japan) was applied to investigate the microstructure and the catalyst morphology. The crystalline structures of the acquired samples were analyzed using X-ray diffraction (XRD; Rigaku D/MAZX 2500 V/PC high-power diffractometer, Tokyo, Japan) with a Cu Kα X-ray source with a wavelength of $\lambda = 1.5415$ Å at a scan rate of 2° (2θ)/min. Fourier transform infrared spectroscopy was used to characterize the functional groups of the produced photocatalysts (FT-IR; Nicolet 380 spectrometer, Thermo Scientific Nicolet iS5 with an iD1 transmission accessory, Waltham, MA, USA). X-ray photoelectron spectroscopy was used to investigate the composition, chemical state, and electronic state of the elements on the Thermo scientific K-Alpha system (XPS, Waltham, MA, USA). A zeta potential analyzer was used to carry out the zeta potential analysis (Zetasizer Nano ZS, Malvern Panalytical, Malvern, United Kingdom). UV-Vis absorption spectra (Specord 210 Plus, AnalytikJena, Germany) and UV–vis diffuse reflectance spectra (SCINCO S-4100 Diffuse Reflectance-Ultraviolet/Visible Spectrophotometer, SCINCO, Korea) were used to examine the photocatalyst optical

characteristics. Photoluminescence spectroscopy was measured with a 473 nm diode laser at ambient temperature (Agilent Technologies, Cary Eclipse fluorescence spectrophotometer, Santa Clara, CA, U.S.A.). Time-resolved fluorescence (TRPL) spectra were performed under 400 nm laser excitation by an FS5 spectrofluorometer (Edinburgh Instruments Ltd, Livingston, UK). Tri-exponential functions were used to fit the emission decay profiles. The lateral sizes and height profiles of the resulting g-C_3N_4 sheets were measured by commercial atomic force microscopy (AFM, MFP-3D, Asylum Research). The optical images of resultant catalysts were captured using an Olympus laser scanning confocal microscope (LSCM). Raman spectra were obtained by confocal Raman microscopy with a 532 nm wavelength incident laser light (Thermo Scientific). Thermogravimetric analysis (TGA) was measured under an argon atmosphere at a heating rate of 10 ℃ min^{-1} (TGA 550 - TA Instruments).

2-5. Electrochemical measurement

An electrochemical workstation (VSP BioLogic Science Instruments, Seyssinet–Pariset, France) was used to perform electrochemical impedance spectroscopy (EIS) measurements in a standard three-electrode cell under visible light irradiation at room temperature. The EIS was carried out in an open circuit, following a 10-minute delay, with an applied frequency range of 100 kHz to 0.01 Hz at an amplitude of 10 mV and a direct current potential of +0.8 VSCE, as described in our previous report [9].

3. Results and discussion

3-1. Crystal structure and chemical composition

The crystal structure of the as-prepared samples was determined by XRD, Fig. 1(a). The XRD pattern of GO showed a clear peak at 11.0°, which disappeared in the Pt/3D-CN-G sample (the 3D-CN-G structure after photodeposition of Pt nanoparticles) after hydrogen reduction, which confirms the conversion of graphene oxide (GO) to reduced graphene oxide (RGO). The XRD patterns of CNb and Pt/3D-CN3-G7 displayed two peaks at 13.15° and 27.65°, which were assigned to the (100) and (002) crystal planes of g-C_3N_4 (JCPDS 87-1526), corresponding to the in-plane structural packing repeat heptazine motifs and interlayer stacking of conjugated aromatic systems, respectively, demonstrating that the overall structure of g-C_3N_4 was maintained after conjunction with RGO and formation of the 3D structure. Furthermore, a new peak at 24.5° in Pt/3D-CN3-G7 appeared, which is attributed to the d_{002} plane of typically reduced graphene oxide (RGO). Other peaks at 40.1, 47.0, and 68.1° in Pt/3D-CN-G XRD patterns were assigned to the (111), (200), and (220) crystalline planes of the Pt nanoparticles, respectively.

Raman spectroscopy and Fourier transform infrared spectroscopy (FTIR) revealed more information about the sample structures. The Raman spectra confirmed the graphitic-based nature of GO and 3D-CN3-G7 in Fig. 1(b). They exhibited two prominent peaks at 1348 cm^{-1} and 1598 cm^{-1}, belonging to the D and G bands in the graphitic structure of graphene, respectively. Small blue shifts in the positions of D and G bands in the composite compared to GO confirm the reduction of GO in 3D-CN3-G7 and the presence of RGO in the structure. The Raman spectrum for CNb did not show any specific intense peak; rather, it exhibited a broad peak in the area of 1200 to 3200 cm^{-1}. Furthermore, the Raman spectrum of 3D-CN3-G7 proved the presence of both reduced graphene oxide and g-C_3N_4 in the prepared catalyst.

As shown in Fig. 1(c), CNb and 3D-CN3-G7 display similar FTIR spectra, suggesting that the chemical structure of g-C_3N_4 can be well preserved during the synthesis process. The sharp peak at about 811 cm^{-1} and the set of peaks in the region of 900-1800 cm^{-1} belong to the vibrational modes of tris-s-triazine units and heptazine motifs, respectively. Furthermore, the absorbance peak in the region between 3500 and 3000 cm^{-1} is assigned to N-H and the stretching mode of epoxide or hydroxyl groups of g-C_3N_4 nanosheets.

To evaluate the chemical composition of Pt/3D-CN-G, X-ray photoelectron spectroscopy (XPS) and elemental analysis were carried out. As shown in Fig. 2a, the peaks of Pt, N, O, and C were clearly observed in the survey spectrum for the Pt/3D-CN-G catalyst. The Pt4f XPS spectrum for the composite, shown in Fig. 2b, confirms the presence of Pt with the oxidation state +2 at the binding energies of 72.5 and 76.5 eV for $Pt4f_{1/2}$ and $Pt4f_{3/2}$, respectively. In Fig. 2c, the high-resolution C1s spectra of oCN illustrate the typical components of carbon in carbon nitride at 287.6 eV, which can be

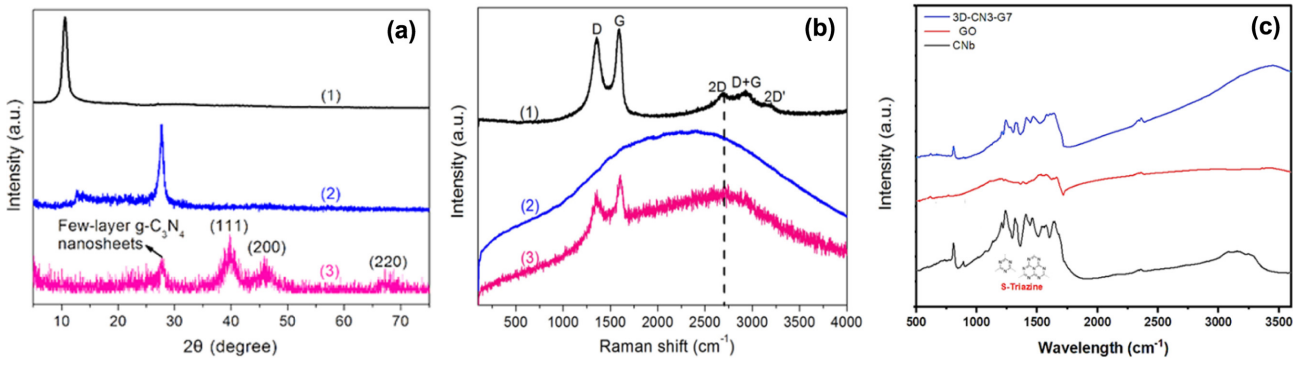

Fig. 1. (a) XRD patterns of (1) GO, (2) CNb, and (3) Pt/3D-CN3-G7 samples, (b) Raman spectra of (1) GO, (2) CNb, and (3) Pt/3D-CN3-G7, and (c) FTIR spectra of Pt/3D-CN3-G7, GO, and CNb samples.

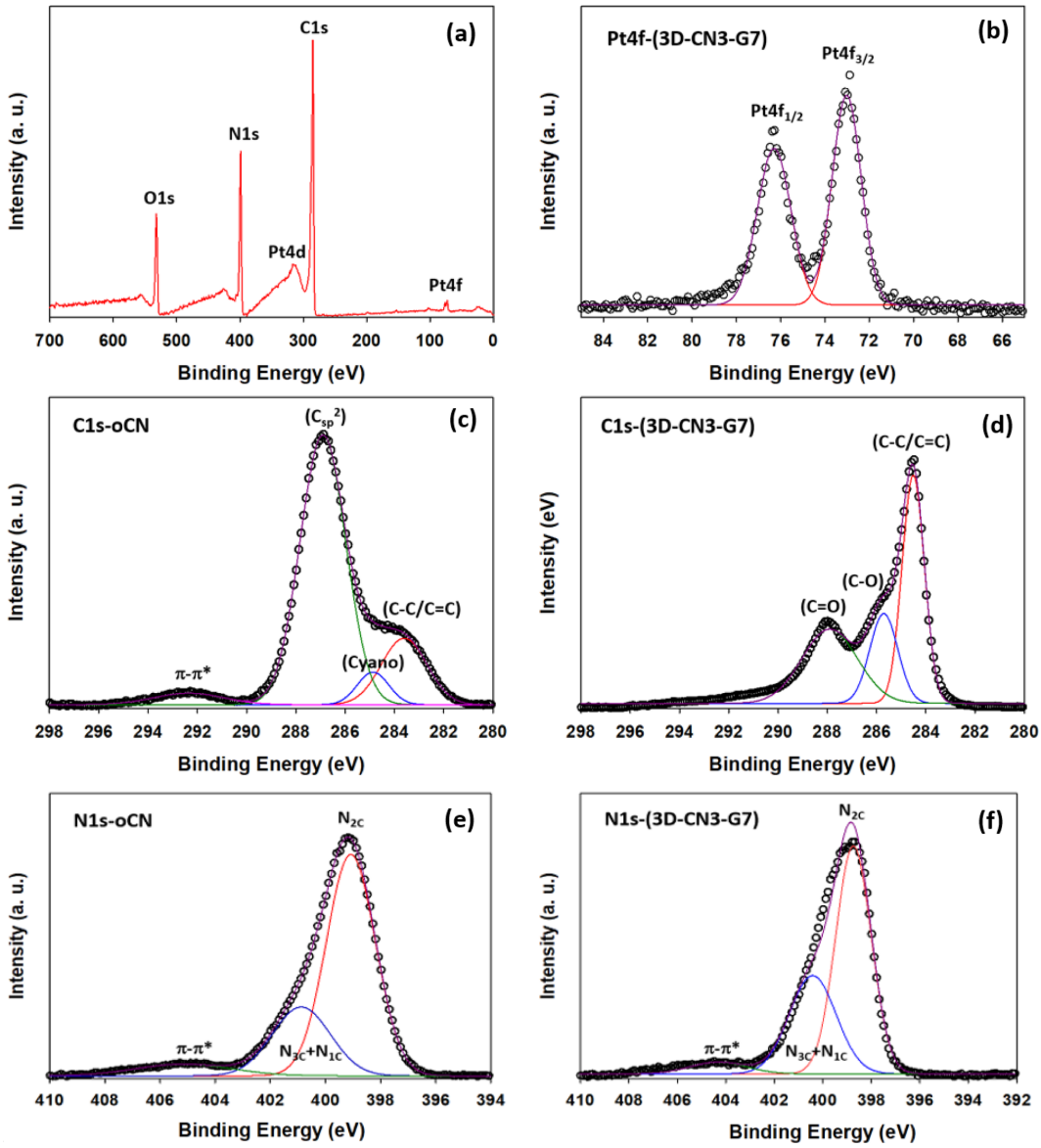

Fig. 2. (a) XPS survey spectra of Pt/3D-CN3-G7, (b) Pt4f region for Pt/3D-CN3-G7, (c) C1s region for oCN, (d) C1s region for Pt/3D-CN3-G7, (e) N1s region for oCN, and (f) N1s region for Pt/3D-CN3-G7.

indexed as C=N bonds. An extra peak around 286.2 eV was assigned to the carbon in cyano groups due to the presence of defect sites in the basal plane of g-C_3N_4. Also, the peak at 284.6 shows the adventitious carbon. The C1s XPS spectrum of the Pt/3D-CN-G (Fig. 2d) indicates the carbon species in the reduced graphene oxide. Since the percentage of RGO is 70% and that of oCN is 30% in the composite, the C-N species belonging to g-C_3N_4 cannot be detected. Also, the degree of GO reduction in the composite system is demonstrated by Fig. 2d. Three components that correspond to C atoms in different functional groups were detected; the highest energy component among them belongs to non-oxygenated ring C-C/C=C at 284.3 eV, which confirms the almost good reduction of GO to RGO in the composite structure. Meanwhile, some oxygenated carbons remain in the structure, including the C atom in the C–O bond at 285.8 eV, and the carbonyl C=O at 288.0 eV. The N1s XPS spectra, Figs. 6e and f, prove the presence of g-C_3N_4 in the composite structure of Pt/3D-CN-G by demonstrating three types of nitrogen similar to those in oCN including N_{2C} (two coordinated nitrogen, N_{sp2}), N_{3C} (three coordinated nitrogen, N_{sp3}), and NH_2 in structures with binding energies of 398.5, 399.8, and 400.6 eV, respectively.

3-2. Surface Morphology

Based on the SEM images, Fig. 3a-f, as the GO content in 3D-CNx-Gy transitioned from 10% to 90%, the morphology of the sample exhibited a significant change. Specifically, the 3D porous aerogel structure started to form when the GO content reached 30%, which implies the critical role of GO in formation of the 3D aerogel motif. Platinum particles size is in a range of 1-10 nm, and typical size is 4 ± 0.5 nm (Fig. 3g-j).

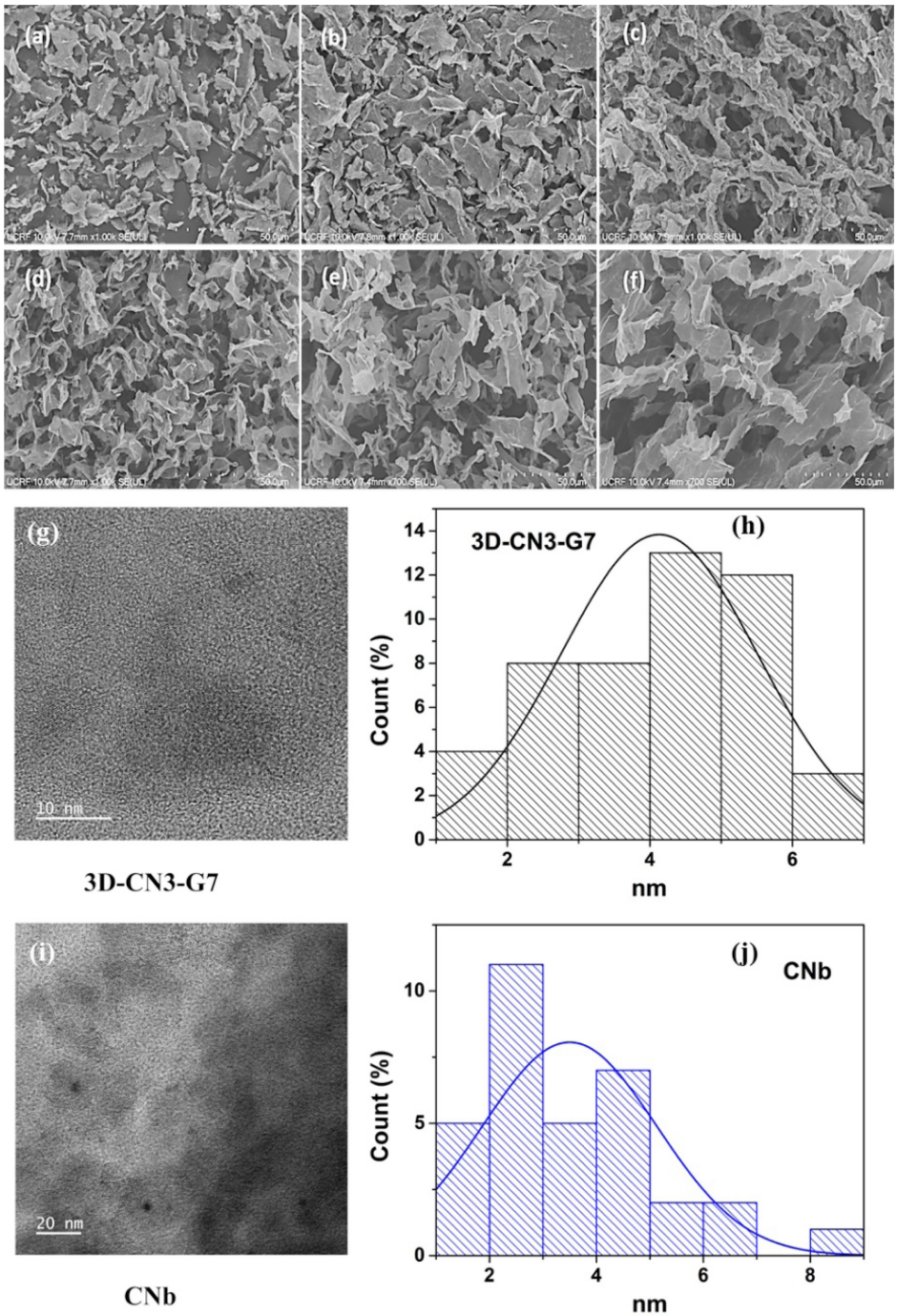

Fig. 3. FESEM images of (a) 3D-CN, (b) 3D-CN9-G1, (c) 3D-CN7-G3, (d) 3D-CN5-G5, (e) 3D-CN3-G7, and (f) 3D-CN1-G9. (g, i) HR-TEM image of CNb and 3D-CN3-G7 samples, corresponding to Pt size distribution (h, j), respectively.

3-3. Optical properties, charge carrier separation and transfer

As shown in Fig. 4a, the UV-Vis spectra present the light absorption regions for 3D-CN3-G7, CNb, and oCN samples. The main absorption peaks for CNb and oCN were located in the UV region ($\lambda < 400$ nm), and their shoulders broadened into visible light range. The bandgap values were determined using Tauc equation [10]:

$$(\alpha h\nu)^{1/n} = A(h\nu - E_g)$$

In which α, h, ν, A, and E_g are the absorption coefficient, frequency of light, proportionality constant, and bandgap energy. Graphitic carbon nitride material is considered to be an indirect bandgap semiconductor with the value of index n in Tauc's equation (1/n=0.5) [11].

The estimated bandgap values (E_g) of as-synthesized g-C_3N_4 were obtained from the intercept of the tangents of the Tauc plot $(\alpha h\nu)^{0.5}$ curve vs. photon energy hν (Figs. 4b, c). The bandgaps of CNb and oCN were calculated to be 2.8 eV and 3.0 eV, respectively. The 3D-CN3-G7 composite can absorb the whole spectrum of light from 300

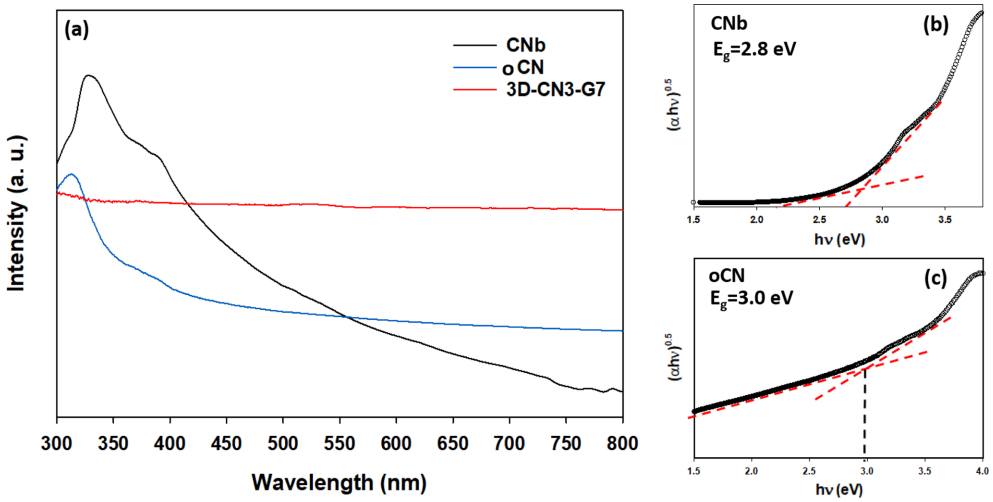

Fig. 4. (a) UV-Vis spectra of 3D-CN3-G7, CNb, and oCN. Corresponding Tauc plots of E (eV) vs. $(\alpha hv)^2$ are shown for (b) CNb, (c) oCN.

to 800 nm, as demonstrated by the UV-Vis absorption spectra, and because its color was completely black.

The recombination, separation, migration and transfer of the photogenerated charge carriers represent the most fundamental aspects of all photocatalytic reactions [12]. To elucidate those phenomena, steady state photoluminescence spectroscopy (PL), electrochemical impedance spectroscopy (EIS), and time-resolved photoluminescence spectroscopy (TR-PL) were utilized to study the properties of the photoinduced electron-hole pairs at the surface of the catalysts, Fig. 5. The PL spectra of the as-synthesized CNb and 3D-CN-G were analyzed with an excitation wavelength of 350 nm [13]. CNb displayed a stronger fluorescence intensity, showing the high possibility for charge recombination. A significant decrease in peak intensity was observed for 3D-CN-G, indicating the successful suppression of photoinduced charge recombination due to the enhanced charge separation and transfer rate and reduced charge diffusion length due to the 3D structure of the photocatalyst, Fig. 5a.

Charge carriers' recombination processes can happen through four recombination mechanisms: band-to-band, trap-assisted in bulk, Auger, and surface recombination. Under 420 nm laser excitation, TR-PL decay spectra were measured to evaluate the radiative and non-radiative recombination of photoinduced electron-hole pairs. The decay rate was calculated using a well-fitted triexponential decay function with three excited-state lifetimes and their respective percentages, Fig. 5c. 3D-CN3-G7 exhibits a longer decay period of 3.39 ns compared to 2.96 ns for oCN and 2.54 ns for CNb, indicating the greater charge separation and slower transfer rate in the structure.

To evaluate the charge transfer process at the catalyst-solution interface, electrochemical impedance spectroscopy (EIS) was conducted. The 3D-CN3-G7 exhibited a smaller arc radius for the Nyquist plot than that of CNb and oCN, Fig. 5b, indicating a reduced resistance for the charge transfer from the catalyst surface to the reactant molecules because of the presence of reduced graphene oxide in the structure. According to the charge transfer facilitation at the interface, the macro and mesoporous structure of 3D-CN3-G7 photocatalyst does not act as a recombination center, rather, the structure provides accessible active sites for charge carriers to catch the reactant molecules easily.

3-4. Photocatalytic performance

Photocatalytic activity toward hydrogen evolution reaction was measured to assess the photocatalytic performance of the as-prepared

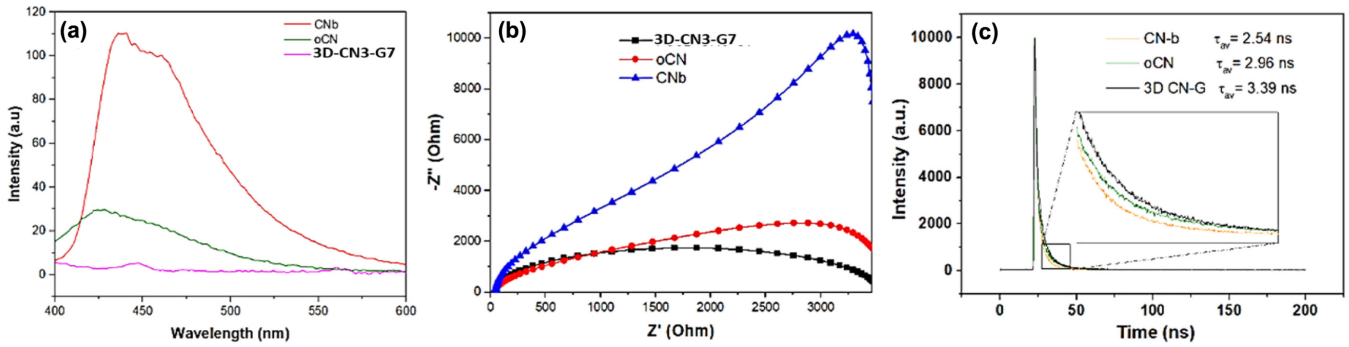

Fig. 5. (a) PL emission spectra, (b) EIS Nyquist plots, and (c) TRPL spectra for CNb, oCN, and 3D-CN3-G7 samples.

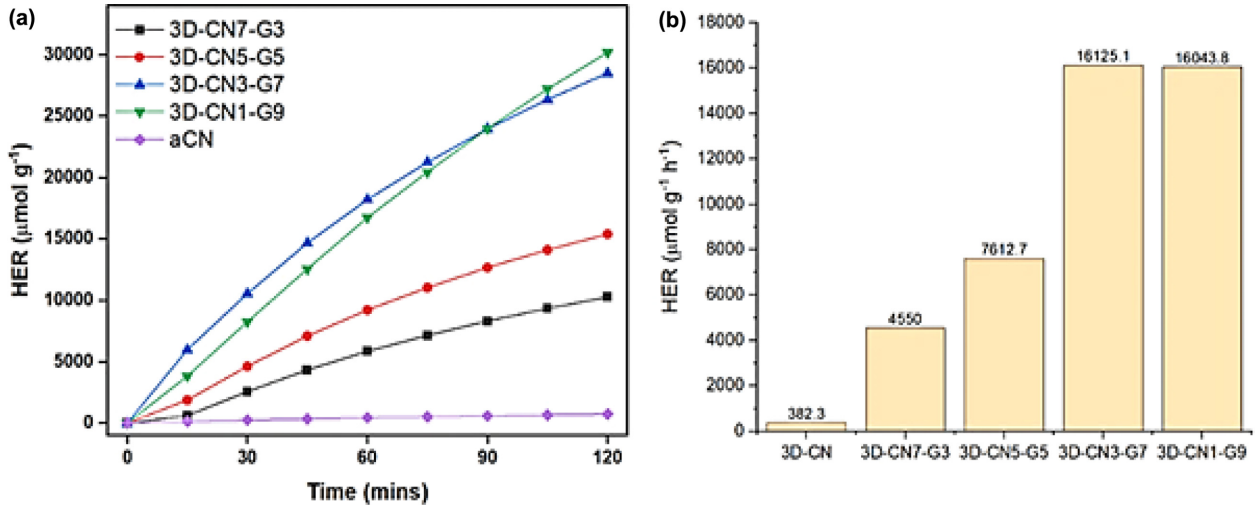

Fig. 6. The effect of RGO content in 3D-CNx-Gy composites on (a) photocatalytic H_2 evolution trend, and (b) photocatalytic H_2 evolution rate.

Table 1. Comparison of photocatalytic activity toward H_2 evolution of the reported g-C_3N_4 and graphene/g-C_3N_4 composites

Materials	Co-catalyst	Light source	Light Intensity (mW cm^{-2})	Hydrogen evolution rate (μmol h^{-1} g^{-1})
3D-CN3-G7 This work	Pt, 3%	300W Xenon (Asashi, Solar mirror)	100	16125.1
SGCN-x [14]	Pt, 2%	300 W Xe lamp (λ ≥ 420 nm)	NR	7446
3D PCN/GO-AAB [15]	None	300 W Xe lamp (λ ≥ 420 nm)	NR	3690
C_3N_4-THF [9]	Pt, 2.3%	Simulated sunlight (Newport, LHS-7320)	100	31256.9
hCN-G [16]	Pt, 1.8%	Simulated sunlight (Newport, LHS-7320)	100	16832.9
NiCoP/g-C_3N_4 [17]	NiCoP	300 W Xe lamp (λ ≥ 420 nm)	NR	1430
EY-mpg-C_3N_4 [18]	Pt, 1 wt.%	300 W Xe lamp (λ ≥ 420 nm)	NR	3850

photocatalysts in the presence of 10% triethanolamine (TEOA) as a sacrificial agent under 300 W Xenon lamp irradiation (λ > 420 nm). Platinum nanoparticles were deposited as the co-catalyst through photodeposition of $H_2PtCl_6 \cdot 6H_2O$. The Pt percentage was controlled at about 3 wt% based on the photocatalyst weight. Eosin Y was added to the solution as a photosensitizer with a mass ratio of 1:1 to the catalyst. As seen in Fig. 6, by increasing the graphene ratio in the 3D composite structure, a higher photocatalytic hydrogen evolution rate was obtained. Both 3D-CN3-G7 and 3D-CN1-G9 showed high enough values of around 16100 $mmol \cdot g^{-1} \cdot h^{-1}$. They also exhibited nearly similar trends in 2 h photocatalytic reaction. As compared, the H_2 evolution performance of graphene-based g-C_3N_4 composites and recent various g-C_3N_4-based materials in the literature is listed in Table 1. Based on the FESEM images, the 3D aerogel structure in the composite started to form well when the amount of graphene reached 50% in the composite, GO (50%): CN (50%). For the samples with higher ratios, better 3D aerogel motifs formed. The porous three-dimensional structure of the composite will provide greater accessibility for the reactants to catch the catalyst active sites to run the reaction. The mass transfer will be facilitated through it. Also, the 3D structure of graphene aerogel provides multidimensional electron transport pathway, which leads to higher charge separation and transfer, resulting in higher photocatalytic activity.

4. Conclusion

We successfully constructed Pt nanoparticle-decorated 3D architectures out of graphene and graphitic carbon nitride nanosheets via a simple and cost-effective EDA-mediated method. The resulting Pt/3D-CN3-G7 hybrid photocatalyst shows excellent photocatalysis for H_2 evolution due to the distinct textural characteristics, such as the 3D interlinking porous structure, high surface area, narrower bandgap, increase in light-harvesting capacity, and good electrical conductivity. The photocatalytic H_2 evolution achieved was as high as 16125.1 $mmol \cdot g^{-1} \cdot h^{-1}$ under visible light irradiation, over 161 times higher than that of bulk g-C_3N_4. Therefore, this 3D hybrid structure may be utilized not only for applications involving recyclable photocatalysts in solution or gas phase, but also as preliminary building blocks suitable for mass production of photocatalytic composites for green hydrogen production.

Acknowledgments

This study was supported by the Regional Innovation Strategy (RIS) through the Ministry of Education (MOE) (2021RIS-003).

References

1. Mohr, S., Wang, J., Ellem, G., Ward, J. and Giurco, D., "Projection of World Fossil Fuels by Country," *Fuel*, **141**, 120-135(2015).
2. Arutyunov, V. S. and Lisichkin, G. V., "Energy Resources of the 21st Century: Problems and Forecasts. Can Renewable Energy Sources Replace Fossil Fuels?," *Russian Chemical Reviews*, **86**(8), 777(2017).
3. O1uyang, X. and Lin, B., "Impacts of Increasing Renewable Energy Subsidies and Phasing Out Fossil Fuel Subsidies in China," *Renewable and Sustainable Energy Reviews*, **37**, 933-942(2014).
4. Wang, X., Maeda, K., Thomas, A., Takanabe, K., Xin, G., Carlsson, J. M., Domen, K. and Antonietti, M., "A Metal-free Polymeric Photocatalyst for Hydrogen Production from Water Under Visible Light," *Nature Materials*, **8**(1), 76-80(2009).
5. Niu, P., Zhang, L., Liu, G., Cheng, H. M., "Graphene-like Carbon Nitride Nanosheets for Improved Photocatalytic Activities," *Advanced Functional Materials*, **22**(22), 4763-4770(2012).
6. Yang, S., Feng, X., Wang, X. and Müllen, K., "Graphene-based Carbon Nitride Nanosheets as Efficient Metal-free Electrocatalysts for Oxygen Reduction Reactions," *Angewandte Chemie*, **123**(23), 5451-5455(2011).
7. Balandin, A. A., Ghosh, S., Bao, W., Calizo, I., Teweldebrhan, D., Miao, F. and Lau, C. N., "Superior Thermal Conductivity of Single-layer Graphene," *Nano Letters*, **8**(3), 902-907(2008).
8. Liu, X. and Dai, L., "Carbon-based Metal-free Catalysts," *Nature Reviews Materials*, **1**(11), 1-12(2016).
9. Dang, T. T., Nguyen, T. K. A., Bhamu, K. C., Mahvelati-Shamsabadi, T., Van, V. K. H., Shin, E. W., Chung, K.-H., Hur, S. H., Choi, W. M., Kang, S. G. and Chung, J. S., "Engineering Holey Defects on 2D Graphitic Carbon Nitride Nanosheets by Solvolysis in Organic Solvents," *ACS Catalysis*, **12**(21), 13763-13780(2022).
10. Cai, L., Hu, J., Li, M. and Yin, P., "Hybrid Catalysts of Molybdovanadophosphoric Acid and g-C_3N_4 with Tunable Bandgaps," *Dalton Transactions*, **49**(31), 10724-10728(2020).
11. Babu, P., Mohanty, S., Naik, B. and Parida, K., "Serendipitous Assembly of Mixed Phase $BiVO_4$ on B-Doped g-C_3N_4: An Appropriate p–n Heterojunction for Photocatalytic O_2 Evolution and Cr(VI) Reduction," *Inorganic Chemistry*, **58**(18), 12480-12491 (2019).
12. Tonda, S., Kumar, S., Kandula, S. and Shanker, V., "Fe-doped and -Mediated Graphitic Carbon Nitride Nanosheets for Enhanced Photocatalytic Performance Under Natural Sunlight," *J. Materials Chemistry A*, **2**(19), 6772-6780(2014).
13. Niu, P., Zhang, L., Liu, G. and Cheng, H.-M., "Graphene-Like Carbon Nitride Nanosheets for Improved Photocatalytic Activities," *Advanced Functional Materials*, **22**(22), 4763-4770(2012).
14. Lei, Z., Yi, Z., Xianghui, Z., Feng, X., Wei, F., Xuan, H., Weixin, L., Xing, D., Daheng, W. and Hui, C., "In-situ Prepare Graphene/g-C_3N_4 D-π-A In-plane Heterojunctions for High-performance Photocatalytic Hydrogen Production," *International J. Hydrogen Energy*, **48**(53), 20290-20302(2023).
15. Li, W., Wang, X., Li, M., He, S.-A., Ma, Q. and Wang, X., "Construction of Z-scheme and p-n Heterostructure: Three-dimensional Porous g-C_3N_4/graphene Oxide-Ag/AgBr Composite for High-efficient Hydrogen Evolution," *Applied Catalysis B: Environmental*, **268**, 118384(2020).
16. Dang, T. T., Bhamu, K. C., Mahvelati-Shamsabadi, T., Oanh Nguyen, T. K. Shin, E. W., Chung, K.-H., Hur, S. H., Choi, W. M., Kang, S. G., Chung, J. S., "Oxidized Platinum Cocatalyst and Self-Assembled Graphene over Graphitic Carbon Nitride for Photocatalytic Hydrogen Evolution," *ACS Applied Nano Materials*, **6**(11), 9825-9838(2023).
17. Li, C., Wu, H., Du, Y., Xi, S., Dong, H., Wang, S. and Wang, Y., "Mesoporous 3D/2D NiCoP/g-C_3N_4 Heterostructure with Dual Co–N and Ni–N Bonding States for Boosting Photocatalytic H_2 Production Activity and Stability," *ACS Sustainable Chemistry & Engineering*, **8**(34), 12934-12943(2020).
18. Min, S. and Lu, G., "Enhanced Electron Transfer from the Excited Eosin Y to mpg-C_3N_4 for Highly Efficient Hydrogen Evolution under 550 nm Irradiation," *J. Physical Chemistry C*, **116**(37), 19644-19652(2012).

Authors

Thi Kieu Oanh Nguyen: Master, Department of Chemical Engineering, University of Ulsan, Ulsan 44610, Korea, kieuoanh896nt@gmail.com

Thanh Truong Dang: Doctor, Department of Chemical Engineering, University of Ulsan, Ulsan 44610, Korea, michael.dang@live.com

Tahereh Mahvelati-Shamsabadi: Doctor, Department of Chemical Engineering, University of Ulsan, Ulsan 44610, Korea, tahereh.mahvelati@gmail.com

Jin Suk Chung: Professor, Department of Chemical Engineering, University of Ulsan, Ulsan 44610, Korea, jschung@ulsan.ac.kr